

## Article

# Effects of Laser-Remelting on the Microstructure, Hardness and Oscillating Wear Resistance of Atmospheric Plasma Sprayed Alumina-Rich Coatings

Maximilian Grimm , Thomas Lindner  and Thomas Lampke 

Materials and Surface Engineering Group, Institute of Materials Science and Engineering, Chemnitz University of Technology, 09107 Chemnitz, Germany; th.lindner@mb.tu-chemnitz.de (T.L.); thomas.lampke@mb.tu-chemnitz.de (T.L.)

\* Correspondence: maximilian.grimm@mb.tu-chemnitz.de

**Abstract:** Thermally sprayed ceramic coatings such as alumina have a specific microstructure characterized by porosity and microcracks. In addition, a process-related phase transformation from  $\alpha$ -Al<sub>2</sub>O<sub>3</sub> to  $\gamma$ -Al<sub>2</sub>O<sub>3</sub> typically occurs, which affects the properties of the coatings compared to sintered alumina. In a previous study, simultaneous additions of Cr<sub>2</sub>O<sub>3</sub> and TiO<sub>2</sub> have already extended and improved the property profile of pure alumina coating (i.e., sliding wear resistance and corrosion resistance against 1N H<sub>2</sub>SO<sub>4</sub>). Depending on the powder material used, the phase composition of the coatings differs considerably, influencing the property profile. Chemical integration through reactive bonding promises a previously untapped potential for improvement. In this study, these alumina-rich ternary oxide coatings are remelted by laser, and the effect of different parameters such as speed, laser power or distance on the macro- and microstructure of the coatings is investigated. For this purpose, both light microscopic and SEM examinations are used as well as the determination of the phase composition by XRD and element distribution by EDS. The created coating microstructures are studied with respect to hardness and oscillation wear resistance.

**Keywords:** atmospheric plasma spray (APS); laser-remelting; alumina; microstructure; wear resistance



**Citation:** Grimm, M.; Lindner, T.; Lampke, T. Effects of Laser-Remelting on the Microstructure, Hardness and Oscillating Wear Resistance of Atmospheric Plasma Sprayed Alumina-Rich Coatings. *Coatings* **2022**, *12*, 721. <https://doi.org/10.3390/coatings12060721>

Academic Editor: Xiujie He

Received: 29 April 2022

Accepted: 17 May 2022

Published: 24 May 2022

**Publisher's Note:** MDPI stays neutral with regard to jurisdictional claims in published maps and institutional affiliations.



**Copyright:** © 2022 by the authors. Licensee MDPI, Basel, Switzerland. This article is an open access article distributed under the terms and conditions of the Creative Commons Attribution (CC BY) license (<https://creativecommons.org/licenses/by/4.0/>).

## 1. Introduction

Thermally sprayed alumina coatings are used in a wide variety of applications, such as wear protection and electrical insulation, due to their high hardness and excellent dielectric strength [1–4]. The high melting temperature and low thermal conductivity of alumina result in a high difficulty of melting factor (DMF) [5,6]. Therefore, atmospheric plasma spraying process (APS) is most commonly utilized for deposition. Other thermal spray processes with lower amounts of thermal energy used for manufacturing alumina coatings are flame spraying, high velocity oxy-fuel (HVOF) spraying and detonation gun spraying (DGS) [7–10]. In all spraying processes, pure alumina shows a specific material behavior. Caused by the high cooling rates of the particles and a lower nucleation energy, a phase transformation takes place. While  $\alpha$ -Al<sub>2</sub>O<sub>3</sub> (corundum) is present in the powdered feedstock, the thermal sprayed coating consists predominantly of the metastable  $\gamma$ -Al<sub>2</sub>O<sub>3</sub> phase [11–14]. The presence of  $\gamma$ -Al<sub>2</sub>O<sub>3</sub> is generally assumed as the main reason that some alumina coating properties, such as corrosion resistance or electrical insulation, are noticeably worse than the properties of sintered alumina [1,15,16]. Retransformation of metastable  $\gamma$ -Al<sub>2</sub>O<sub>3</sub> to favored  $\alpha$ -Al<sub>2</sub>O<sub>3</sub> can be reached through heat treatment or service temperature above 900 °C, with complete transformation occurring at 1200 °C [17–19]. Due to the density differences between  $\gamma$ -Al<sub>2</sub>O<sub>3</sub> and  $\alpha$ -Al<sub>2</sub>O<sub>3</sub> as well as the large thermal stress caused by the high temperatures required, this phase retransformation is often related to extensive formation of defects in the coating, deterioration of the substrate

properties or damage to the coating–substrate interface due to different thermal expansion coefficients [17,18,20].

Laser-remelting is a promising approach to realize the retransformation of  $\alpha$ -Al<sub>2</sub>O<sub>3</sub> and to improve the coating properties with a minimum of thermal stress on the coating–substrate composite [21–24]. In addition, in laser-remelted Al<sub>2</sub>O<sub>3</sub>-TiO<sub>2</sub> coatings, the formation of Al<sub>2</sub>TiO<sub>5</sub> was observed [22,23]. In general, APS coatings treated by laser-remelting show a dense and homogeneous zone but often also larger defects such as cracks as a result of the stresses [21,25–28]. After laser-remelting, the roughness of the coatings is reduced compared to the as-sprayed state [23]. Several studies show that laser-remelting can improve both the hardness and wear resistance of alumina coatings [23,24,26].

Additions of TiO<sub>2</sub> or Cr<sub>2</sub>O<sub>3</sub> can diversify the property profile and improve performance compared to plain alumina coatings. TiO<sub>2</sub> additions lead to better melting behavior of the powder particles and thus improve the deposition efficiency and overall microstructure of the coating [29,30]. As a result of the reduced porosity and cracking of the coating, an increase in fracture toughness is often reported [31–33]. Both the lower defect level in the microstructure and the higher fracture toughness also enhance the wear resistance of Al<sub>2</sub>O<sub>3</sub>-TiO<sub>2</sub> coatings under certain test conditions [30,33]. Cr<sub>2</sub>O<sub>3</sub> additives, however, can improve wear resistance due to their extreme hardness. By forming an (Al,Cr)<sub>2</sub>O<sub>3</sub> solid solution, depending on the chromium content, stabilization of the  $\alpha$ -phase can be realized during the spraying process [13,14]. For both Cr<sub>2</sub>O<sub>3</sub> and TiO<sub>2</sub> additives, the effect on the actual property profile depends strongly on the type of feedstock powder used and the coating microstructure present. In a previous study, the influence of the simultaneous Cr<sub>2</sub>O<sub>3</sub> and TiO<sub>2</sub> additions on the microstructure and property profile of alumina-rich coatings was investigated in more detail [29]. Since these coating systems serve as the starting point for the present study, it is strongly recommended in order to achieve a better understanding.

The aim of the current study was to investigate the capability of laser-remelting to improve the wear properties of such multi-component coatings and to analyze the effects of different laser-remelting process parameters on the micro- and macrostructure of the coating. For this purpose, alumina-rich coatings (81.0 wt% Al<sub>2</sub>O<sub>3</sub>, 12.5 wt% Cr<sub>2</sub>O<sub>3</sub>, 6.5 wt% TiO<sub>2</sub>) are prepared using APS in the same way as in a previous study [29]. Despite the identical chemical composition, the coatings differ considerably in terms of their microstructure and properties. These coatings are remelted using a multi-diode laser, and the effect of different parameters of the laser process, such as power and velocity, on the macro- and microstructure and tribological properties of the coatings is investigated. Particular attention is also paid to the possibility of converting the multiphase coatings into single-phase coatings by reactions between the individual lamellae due to laser-remelting.

## 2. Materials and Methods

In this paper, three alumina-rich coatings are studied, having nominally the same chemical composition (81 wt% Al<sub>2</sub>O<sub>3</sub>, 12.5 wt% Cr<sub>2</sub>O<sub>3</sub>, 6.5 wt% TiO<sub>2</sub>), but differing in microstructure with regard to their porosity phase composition (i.e., blend so: multi-phase and as1: single-phase solid solution structure) and elemental distribution. For this purpose, two powder blends of fused and crushed powders were prepared, and one experimental powder feedstock was produced by agglomeration and sintering (hereinafter referred to as “as1”). The two powder blends consisted of the three single oxides (hereinafter referred to as “blend so”) and of an Al<sub>2</sub>O<sub>3</sub>-25 wt% Cr<sub>2</sub>O<sub>3</sub> and an Al<sub>2</sub>O<sub>3</sub>-13 wt%TiO<sub>2</sub> powder (hereinafter referred to as “blend bfc”). The feedstock powders used, the specification of the deposition by APS, and the microstructure and properties of the coatings are described in detail in a previous study [29]. In this study, these three coating systems were used to investigate the effect of laser-remelting on the microstructure and properties. Before laser-remelting, the coatings were ground and polished to produce a more comparable surface condition (roughness). A smooth surface is also essential for the determination of the vibration wear resistance. A multi-diode laser (Laserline, Lunov, Herzogenrath, Germany) operating with a wavelength of 980 nm was used for laser-remelting. The working distance was

constant at 20 mm, representing the focus spot of the laser, which has a diameter of 5 mm. The heat input into the coatings was varied by adjusting the laser power (150–450 W) and traverse speed (0.5–20 mm/s). Table 1 shows the parameter sets and the corresponding characteristic values used to obtain the best results without delamination for the respective coating types.

**Table 1.** Parameter sets used for laser-remelting of ternary oxide coatings.

System	Laser Power $P_{el}$ (W)	Traverse Speed $v$ (mm/s)	Energy Density <sup>1</sup> (J/mm <sup>2</sup> )
as1 ((Al,Cr,Ti) <sub>2</sub> O <sub>3</sub> )	225	1	45
blend bfc ((Al,Cr) <sub>2</sub> O <sub>3</sub> + Al <sub>2</sub> O <sub>3</sub> – TiO <sub>2</sub> )	200	1	40
blend so (Al <sub>2</sub> O <sub>3</sub> + Cr <sub>2</sub> O <sub>3</sub> + TiO <sub>2</sub> )	300	10	6

<sup>1</sup> Energy density J is calculated from  $J = P_{el}/(v \cdot D)$  [24]; D: diameter focus point.

Cross sections were prepared using standard metallographic methods. For the evaluation of the laser-remelted tracks, images of the surface were taken using a stereo microscope MVX10 equipped with a UC90 camera (Olympus, Tokyo, Japan), and the microstructure was analyzed by scanning electron microscope (SEM) (LEO 1455VP, Zeiss, Oberkochen, Germany) using an acceleration voltage of 25 kV and backscattered electron detector (BSD). In addition, EDS analysis (GENESIS, EDAX, Mahwah, NJ, USA) was used to determine both the average chemical composition of the laser-remelted zone and the local chemical composition of the characteristic areas. To determine the average coating composition, large regions of the cross section (250  $\mu$ m  $\times$  30  $\mu$ m) were measured at three randomly selected locations. The local chemical composition of the characteristic areas was studied by five measuring points. The phase composition was studied by X-ray diffraction (XRD) using a D8 Discover diffractometer (Bruker AXS, Billerica, MA, USA) with a point focus (0.5 mm) operating with Co K $\alpha$  radiation, a tube voltage of 35 kV, and a tube current of 40 mA. The diffraction patterns were measured for a  $2\theta$  range from 20° to 130° with a step size of 0.03° and a dwell time of 10.2 s/step.

The Vickers microhardness of the coatings was measured on the surface of the laser-remelted tracks by ten indentations with a test load of 2.94 N performed using a Wilson Tukon 1102 device (Buehler, Uzwil, Switzerland).

The wear resistance of the laser-remelted coatings was evaluated by an oscillating wear test according to ASTM G133, in which the counterbody (Al<sub>2</sub>O<sub>3</sub> ball: 10 mm diameter, grade 10) was pushed against the oscillating moving sample with a defined test force. All test parameters are summarized in Table 2. Three repetitions were performed for each specimen. An optical 3D profilometer MikroCAS (LMI, Teltow, Germany) was used to determine the volume of the resulting wear marks.

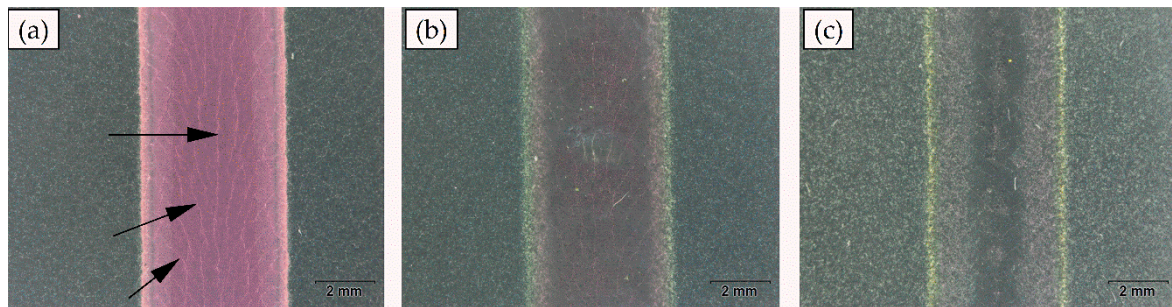
**Table 2.** Parameters of oscillating wear test.

Force (N)	Frequency (Hz)	Time (s)	Amplitude (mm)	Counterbody	
				Material	Diameter (mm)
16	40	600	0.5	Al <sub>2</sub> O <sub>3</sub>	10

### 3. Results

Figure 1 shows the images of surfaces of the laser-remelted tracks captured by a stereomicroscope. The tracks have a width of 5 mm, which corresponds to the diameter of the focus spot of the laser used. The red coloring of the laser-remelted track of the “as1” coating (Figure 1a) is particularly noticeable, whereas only a slight change in color

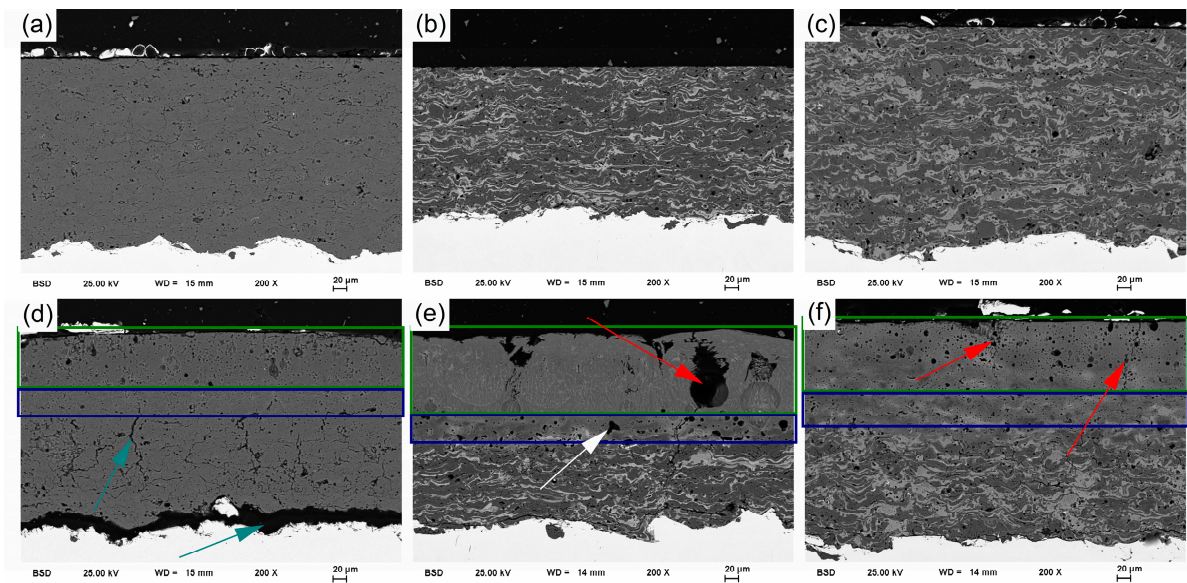
can be observed for the laser-remelted tracks on the “blend bfc” (Figure 1b) and “blend so” (Figure 1c) coatings. Furthermore, it is noticeable that the coloring of the remelted tracks is not uniform but loses color intensity toward the edge. The transition to the initial thermally sprayed coating is clearly recognizable in all laser-remelted tracks by a thin, light coloration. In addition, severe cracks can be seen running parallel to the laser movement in the center of the track. Toward the edge, the cracks run increasingly perpendicular to the laser movement.



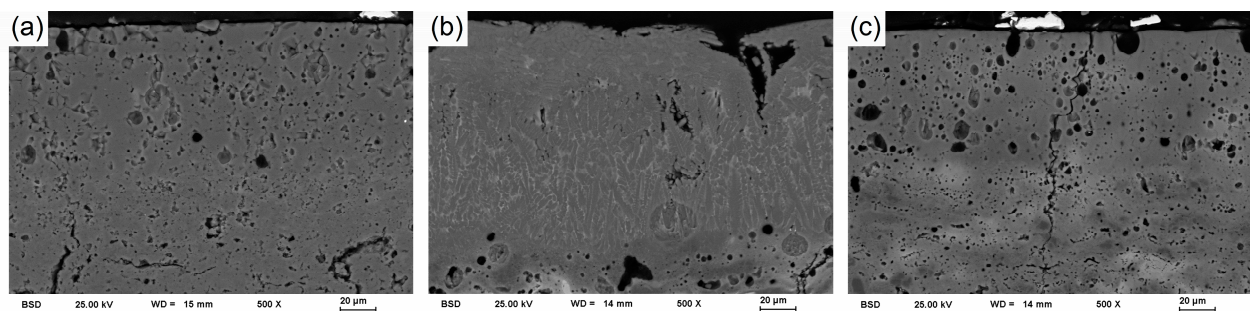
**Figure 1.** Top-view images of the laser-remelted tracks of the coatings: (a) as1, (b) blend bfc, (c) blend so, with severe cracks in the direction of laser movement (black arrows).

Figure 2 presents the SEM images of cross sections of the coatings before (a–c) and after laser-remelting (d–f). In the original state (Figure 2a–c), the coatings possess characteristics typical of thermally sprayed coatings, such as low porosity and some microcracks located along the splat boundaries or within the splats. Corresponding to the feedstock powder used, the coatings differ considerably in their phase composition. Whereas the “blend so” and “blend bfc” coatings, made from powder blends, are multiphase, the “as1” coating is largely single-phase due to the formation of an  $(Al,Cr,Ti)_2O_3$  solid solution. Detailed analysis of the microstructures and properties of these coatings have already been presented in a previous study [29]. The present study is focused on the changes obtained by laser-remelting. Figure 2d–f shows the selected laser-remelted track of the respective coating system, and Figure 3 shows a detailed view of the laser-remelted zone. Significant differences can be observed, especially in the coatings made from powder blends (“blend bfc” and “blend so”).

Within the laser-remelted zone (green rectangles), the coatings no longer possess the characteristic lamellar structure, but have a relatively dense, dendritic microstructure (Figure 3b) in which boundaries of former particles/splats are no longer identifiable. In the laser-remelted zone, these coatings show a uniform shade of gray in BSD contrast. However, the laser-remelted coatings also contain defects, including small and medium pores (Figure 3a,c) and cavities (up to 30  $\mu\text{m}$ ) (Figure 2e, red arrow), which are mostly encapsulated in contrast to the as-sprayed state. In addition, the coatings show more severe and more frequently microcracks both in the laser-remelted zone (Figure 2f, red arrows) and in the surrounding coating (Figure 2d, cyan arrows). In addition, a transition zone (Figure 2d–f, blue rectangles) between the original coating and the laser-remelted zone can be recognized, especially in the coatings made from powder blends. This exhibits structural features that differ from both the original coating structure and the remelted edge of the coating. Furthermore, an accumulation of smaller pores (pore fringe) can be observed in the transition area (Figure 2e, white arrow).



**Figure 2.** SEM images of the cross-sections of the coatings before (upper row) and after (lower row) laser-remelting treatment: (a,d) as1, (b,e) blend bfc and (c,f) blend so. After laser-remelting treatment, coatings show a laser-remelted zone (green rectangle), in which the original lamellar structure is no longer noticeable, and a transition zone (blue rectangle). In both zones and in the original coating underneath, numerous defects such as pores, microcracks or local delamination (marked by arrows) can be found.



**Figure 3.** SEM images (detailed view) of the laser-remelted zone of the coatings: (a) as1, (b) blend bfc and (c) blend so.

The EDS analysis, shown in Figure 4, reveal a uniform distribution of chemical elements in the laser-remelted zone for all coatings. For the coatings made from powder blends (“blend bfc” and “blend so”), this is a particular change compared to the initial state, where the chemical composition of the individual splats differ according to the feedstock powders used. For the “as1” coating, a solid solution structure is already present in the initial state, as an experimental powder produced by agglomeration and sintering was used. Therefore, no significant differences in the chemical composition of the splats and the laser-remelted zone are detected. The average chemical composition of the coatings, as well as the chemical composition of the laser-remelted zones, are similar in the different coating systems. Only slight differences in the average chemical composition, especially with regard to the titanium content, occur in the coating and the laser-remelted zone (i.e., “as1”).

The XRD patterns, illustrated in Figure 5, show that the coatings have different phase compositions depending on the feedstock powder used. The coatings “as1” and “blend bfc” consist mainly of the differing solid solutions  $\alpha$ - and  $\gamma$ -(Al,Cr,Ti)<sub>2</sub>O<sub>3</sub>. The “blend so” coatings do not contain such a solid solution and have only a small proportion of

$\alpha$ -Al<sub>2</sub>O<sub>3</sub>. More detailed descriptions on the phase composition of the coatings as well as the changes compared to the feedstock powders due to the spraying process can be found in a previous study [29]. Conversely, the laser-remelted zones show similar XRD patterns among themselves, where the majority of the peaks can be assigned to an  $\alpha$ -(Al,Cr,Ti)<sub>2</sub>O<sub>3</sub> phase. What remains is a large peak at  $2\theta = 30.8^\circ$  and smaller peaks at  $2\theta = 59.5^\circ$ ,  $69.8^\circ$  and  $71.5^\circ$ . In particular, the dominant peak at  $2\theta = 30.8^\circ$  indicates an A<sub>2</sub>BO<sub>5</sub> type phase with A as the trivalent element (Al<sup>3+</sup>, Cr<sup>3+</sup> or Ti<sup>3+</sup>) and B as the tetravalent Ti<sup>4+</sup>. The structure of the A<sub>2</sub>BO<sub>5</sub> phase is similar to phases Cr<sub>2</sub>TiO<sub>5</sub>, Al<sub>2</sub>TiO<sub>5</sub> or Ti<sub>3</sub>O<sub>5</sub>.

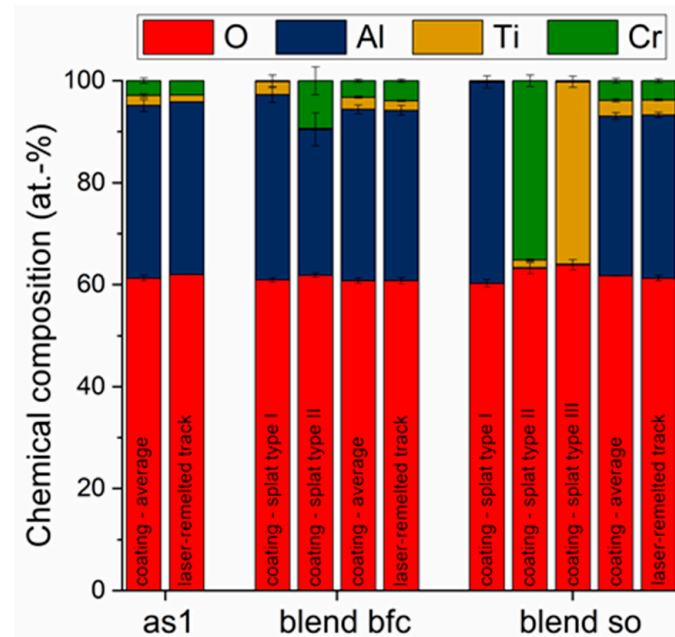


**Figure 4.** EDS analysis of the laser-remelted tracks compared to the initial state of the coatings described in more detail in a previous study [29]. Uniform element distribution and only a slight change in chemical composition (compared to average composition of the coating) due to dissolving and reaction of the individual splats.

From the shifted peak positions of the  $\alpha$ - and  $\gamma$ -phases, the corresponding lattice parameters  $a$  and  $c$ , shown in Figure 6, were determined as an indicator of the incorporation of foreign atoms (exchange solid solution). The  $\gamma$ -phase in coatings “as1” and “blend bfc” show increased values for the lattice parameter  $a$ , while in the “blend so” coating, the lattice parameter  $a$  corresponds to the reference. Remarkably, the same values for lattice parameter  $a$  are determined for the “as1” and “blend bfc” coating. In the “blend so” coating, the lattice parameters  $a$  and  $c$  of the  $\alpha$ -phase also correspond to the reference. The  $\alpha$ -phase of the “as1” coating has larger lattice parameters  $a$  and  $c$ . In the “blend bfc” coating, two  $\alpha$ -phases were detected in the XRD measurements. In one, the lattice parameters correspond to those of the reference, and in the other, much higher values were determined. In the laser-remelted tracks, only for the  $\alpha$ -phase could the lattice parameters be determined, since too few other peaks were detected for the A<sub>2</sub>BO<sub>5</sub>-type phase, except for the dominant peak at  $30.8^\circ$ . The  $\alpha$ -phase of the laser-remelted track on the “as1” coating has similar parameters as in the coating. In the “blend bfc” and “blend so” coatings, laser-remelting leads to an  $\alpha$ -phase with lattice parameters significantly different from those of  $\alpha$ -phases occurring in the coating. The  $\alpha$ -phases in these laser-remelted zones (“blend bfc” and “blend so”) have a high similarity.

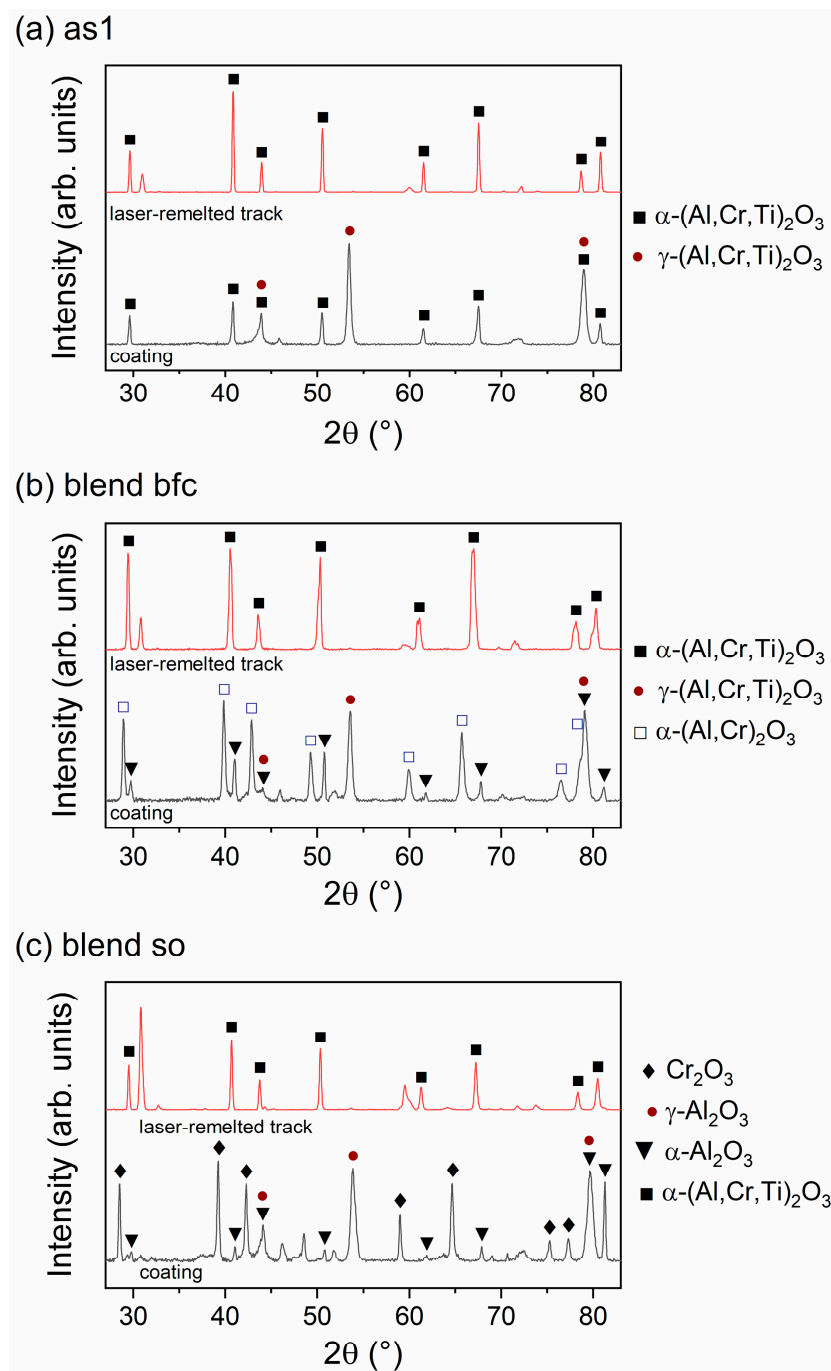


**Figure 5.** Diffraction patterns of initial coating and respective laser-remelted track: (a) as1, (b) blend bfc and (c) blend so.

Figure 7 shows the microhardness and oscillating wear rate of the coatings and remelted tracks. All laser-remelted tracks possess an extremely high hardness on the surface on a comparable level of about 1800–1900 HV0.3. This marks a significant increase compared to the as-sprayed state and is in good agreement with other studies on laser-remelted alumina coatings [24,34]. Laser-remelting also has a positive effect on oscillating wear resistance, with a significant reduction in the wear rate compared to the as-sprayed state. The direct comparison with the literature is difficult due to the dependence of the wear rate on the tested tribological system (i.e., test parameters) and the lack of suitable references. However, studies on sliding wear already indicate an increase in wear resistance as a result of laser-remelting [24,28,35].

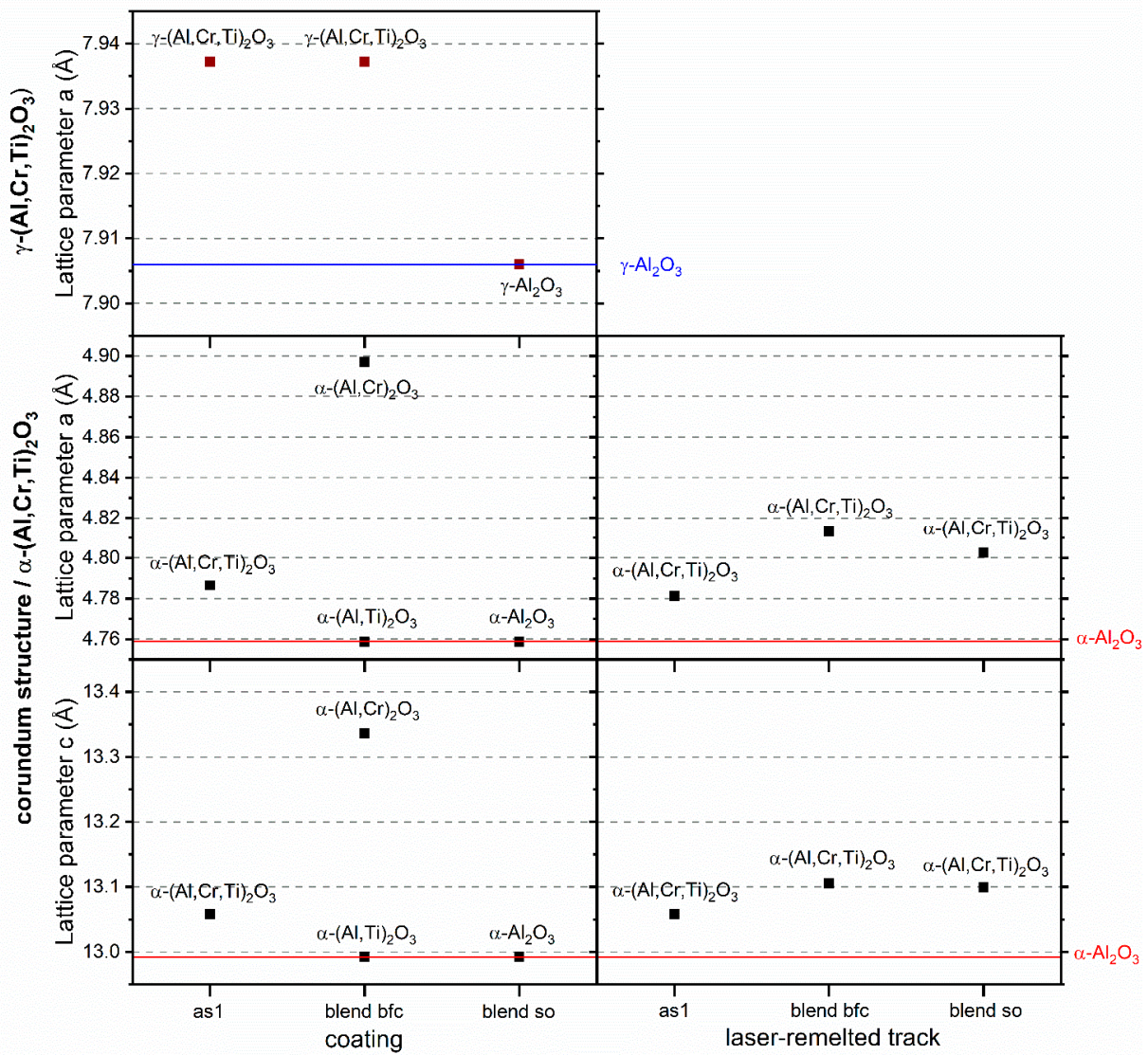


Figure 6. Lattice parameters of the  $\gamma$ - and  $\alpha$ -phases of the coatings (left) and laser-remelted tracks (right). Shift of lattice parameters indicates incorporation of foreign atoms (exchange solid solution).

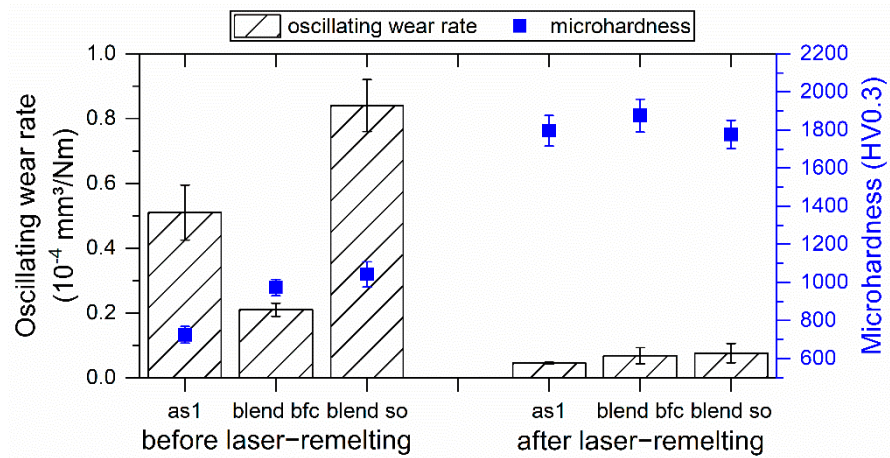


Figure 7. Oscillating wear rate and microhardness of coatings and laser-remelted tracks. Significant improvements due to laser-remelting.

#### 4. Discussion

Laser-remelting of alumina-rich multicomponent coatings using a multi-diode laser leads to a significant change in their microstructure. This becomes especially obvious in the disappearance of the typical lamellar structure of thermally sprayed coatings. As a result of the heat input, the individual lamellae/splats dissolve by reacting with each other, forming new phases that grow in dendritic structures. Despite the short process times, a largely homogeneous laser-remelted zone is formed from previously heterogeneous coating structures (e.g., “blend so”). The formation of these solid solutions can be traced by XRD measurements with determination of the lattice parameters as well as by EDS measurements. Due to the larger ionic radii of  $\text{Cr}^{3+}$  and  $\text{Ti}^{3+}$  (62 and 67 pm, respectively) compared to  $\text{Al}^{3+}$  (54 pm), the incorporation of these atoms into  $\text{Al}_2\text{O}_3$  leads to an increase in the lattice parameters. Thus, the level of change of the lattice parameters indicates the amount of incorporated foreign atoms. Regardless of the phase composition of the coating,  $\alpha\text{-(Al,Cr,Ti)}_2\text{O}_3$  is mainly present after laser-remelting, which already existed in the homogeneous “as1” coating. According to the determined lattice parameters, this phase is similar in all laser-remelted tracks. The slightly smaller lattice parameters for “as1” is a result of the lower proportion of atom replacement, as can be seen in the EDS measurements, which have already taken up a smaller proportion in the coating. Therefore, this lack of Cr and Ti is due to evaporation during powder production. Thus, the loss of an element because of laser-remelting can be excluded. The phase transformation of the  $\gamma$ -phase predominant in the coatings to the  $\alpha$ -phase in the laser-remelted tracks reveals that the cooling rate during laser-remelting is considerably lower than during APS. Therefore, the results are consistent with previous works [21,23,24,27]. However, it has to be assumed that laser-remelting creates high residual stresses leading to defects such as cracks visible in the optical microscope. These residual stresses are likely caused by the high temperature gradient between the laser-remelted zone and the remaining coating. In addition, the residual stresses can be further increased by the volume increase induced by the  $\gamma \rightarrow \alpha$  phase transformation. In addition to the larger cracks, the laser-remelted zone shows other defects. Pores can either cluster as finely dispersed at the interface between the laser-remelted zone and the remaining coating, forming a pore fringe, accumulating into large cavities, forming pits at the surface, or remaining in the laser-remelted zone. When laser-remelting the “as1” coating, a network of cracks appeared in the surrounding coating as well as partial delamination at the coating–substrate interface, probably due to the defect-rich microstructure of the original coating (microcracks along the splat boundaries). A particularly thick and dense (except for large cavities) laser-remelted zone having a dendritic/columnar structure was obtained for the “blend bfc” coating. Despite the nominally identical chemical compositions, the coatings showed strongly different responses to laser treatment depending on their microstructure. All laser-remelted tracks consist of the same phase, but differ in their defect density. Despite the defects, all coatings exhibit superior microhardness, which ranks closer to the level of sintered ceramics than to that of thermally sprayed ceramic coatings. All laser-remelted tracks also show significantly enhanced resistance against oscillation wear compared to the coatings. Increased wear of the counterbody was not observed. Based on the microstructure, it is likely that the high hardness and compact microstructure of the laser-remelted coating contribute to the increase in wear behavior. Detachment or breaking out of individual splats, as occurs in the lamellar structure of thermally sprayed coatings, can be prevented by laser-remelting.

#### 5. Conclusions

In this study, the effects of laser-remelting using a multi-diode laser on microstructure, hardness and oscillating wear of multicomponent alumina-rich coatings were investigated:

- Laser-remelting provides a relatively dense and hard wear-resistant zone.
- The laser-remelted zone has defects (pores), which differ depending on the laser parameters and phase composition of the initial coating.

- In all coatings, the laser remelted zone has a compact structure that exhibits high homogeneity.
- The lamellae/splats of the original coating react with each other and form a solid solution ( $\alpha$ -(Al,Cr,Ti)<sub>2</sub>O<sub>3</sub>) independent of the initial phase composition. Both EDS and XRD measurements indicate the incorporation of the atoms.
- The transformation from  $\gamma$ - (coating) to  $\alpha$ -phase (laser-remelted zone) takes place.
- Volume decrease (phase transformation) and temperature gradient result in high residual stresses, leading to cracks.

In further studies, the formation of defects and the influence of different phases on them have to be investigated in more detail in order to develop methods (such as preheating or using a pulsed CO<sub>2</sub> laser) to reduce the defect density.

**Author Contributions:** Conceptualization, M.G., T.L. (Thomas Lindner) and T.L. (Thomas Lampke); investigation, M.G.; discussion, M.G., T.L. (Thomas Lindner) and T.L. (Thomas Lampke); writing—original draft preparation, M.G.; writing—review and editing, T.L. (Thomas Lindner) and T.L. (Thomas Lampke); supervision, T.L. (Thomas Lampke); project administration, T.L. (Thomas Lampke). All authors have read and agreed to the published version of the manuscript.

**Funding:** The APC was funded by the Deutsche Forschungsgemeinschaft (DFG, German Research Foundation) project number 491193532 and the Chemnitz University of Technology.

**Institutional Review Board Statement:** Not applicable.

**Informed Consent Statement:** Not applicable.

**Data Availability Statement:** Not applicable.

**Acknowledgments:** The authors would like to specifically thank Robert Glaßmann, Marc Pügner, Christian Loos and Niclas Hanisch for their great assistance in the laser-remelting process, metallographic preparation, XRD measurement and wear testing.

**Conflicts of Interest:** The authors declare no conflict of interest.

## References

1. Berger, L.-M. Tribology of Thermally Sprayed Coatings in the Al<sub>2</sub>O<sub>3</sub>-Cr<sub>2</sub>O<sub>3</sub>-TiO<sub>2</sub> System. In *Thermal Sprayed Coatings and Their Tribological Performances*; Roy, M., Davim, J.P., Eds.; IGI Global: Hershey, PA, USA, 2015; pp. 227–267. ISBN 9781466674899.
2. Sampath, S. Thermal Spray Applications in Electronics and Sensors: Past, Present, and Future. *J. Therm. Spray Technol.* **2010**, *19*, 921–949. [[CrossRef](#)]
3. Toma, F.-L.; Scheitz, S.; Berger, L.-M.; Sauchuk, V.; Kusnezoff, M.; Thiele, S. Comparative Study of the Electrical Properties and Characteristics of Thermally Sprayed Alumina and Spinel Coatings. *J. Therm. Spray Technol.* **2011**, *20*, 195–204. [[CrossRef](#)]
4. Mohammadian Bajgiran, M.; Rezvani Rad, M.; McDonald, A.; Moreau, C. Microstructure, phase and dielectric strength of thermally sprayed alumina layers in coating-based heating systems. *Int. J. Appl. Ceram. Technol.* **2021**, *18*, 1641–1656. [[CrossRef](#)]
5. Grimm, M.; Conze, S.; Berger, L.-M.; Paczkowski, G.; Drehmann, R.; Lampke, T. Changes in the coating composition due to aps process conditions for Al<sub>2</sub>O<sub>3</sub>-Cr<sub>2</sub>O<sub>3</sub>-TiO<sub>2</sub> ternary powder blends. *J. Therm. Spray Technol.* **2021**, *30*, 168–180. [[CrossRef](#)]
6. McPherson, R. The relationship between the mechanism of formation, microstructure and properties of plasma-sprayed coatings. *Thin Solid Films* **1981**, *83*, 297–310. [[CrossRef](#)]
7. Habib, K.A.; Saura, J.J.; Ferrer, C.; Damra, M.S.; Giménez, E.; Cabedo, L. Comparison of flame sprayed Al<sub>2</sub>O<sub>3</sub>/TiO<sub>2</sub> coatings: Their microstructure, mechanical properties and tribology behavior. *Surf. Coat. Technol.* **2006**, *201*, 1436–1443. [[CrossRef](#)]
8. Niemi, K.; Vuoristo, P.; Mäntylä, T. Properties of alumina-based coatings deposited by plasma spray and detonation gun spray processes. *J. Therm. Spray Technol.* **1994**, *3*, 199–203. [[CrossRef](#)]
9. Shakhova, I.; Mironov, E.; Azarmi, F.; Safonov, A. Thermo-electrical properties of the alumina coatings deposited by different thermal spraying technologies. *Ceram. Int.* **2017**, *43*, 15392–15401. [[CrossRef](#)]
10. Toma, F.-L.; Stahr, C.C.; Berger, L.-M.; Saaro, S.; Herrmann, M.; Deska, D.; Michael, G. Corrosion resistance of APS- and HVOF-sprayed coatings in the Al<sub>2</sub>O<sub>3</sub>-TiO<sub>2</sub> system. *J. Therm. Spray Technol.* **2010**, *19*, 137–147. [[CrossRef](#)]
11. McPherson, R. Formation of metastable phases in flame- and plasma-prepared alumina. *J. Mater. Sci.* **1973**, *8*, 851–858. [[CrossRef](#)]
12. McPherson, R. On the formation of thermally sprayed alumina coatings. *J. Mater. Sci.* **1980**, *15*, 3141–3149. [[CrossRef](#)]
13. Chráska, P.; Dubsky, J.; Neufuss, K.; Písacka, J. Alumina-base plasma-sprayed materials part I: Phase stability of alumina and alumina-chromia. *J. Therm. Spray Technol.* **1997**, *6*, 320–326. [[CrossRef](#)]
14. Stahr, C.C.; Saaro, S.; Berger, L.-M.; Dubský, J.; Neufuss, K.; Herrmann, M. Dependence of the stabilization of  $\alpha$ -alumina on the spray process. *J. Therm. Spray Technol.* **2007**, *16*, 822–830. [[CrossRef](#)]

15. Gao, J.; Xiong, X.; Gao, Y. The effect of the  $\alpha/\gamma$  phase on the dielectric properties of plasma sprayed  $\text{Al}_2\text{O}_3$  coatings. *J. Mater. Sci. Mater. Electron.* **2017**, *28*, 12015–12020. [[CrossRef](#)]
16. Herrmann, M.; Toma, F.-L.; Berger, L.-M.; Kaiser, G.; Stahr, C.C. Comparative study of the corrosion resistance of thermally sprayed ceramic coatings and their bulk ceramic counterparts. *J. Eur. Ceram. Soc.* **2014**, *34*, 493–504. [[CrossRef](#)]
17. Thompson, V.S.; Whittemore, O.J. Structural changes on reheating plasma-sprayed alumina. *Am. Ceram. Soc. Bull.* **1967**, *46*, 637–641.
18. Heintze, G.N.; Uematsu, S. Preparation and structures of plasma-sprayed  $\gamma$ - and  $\alpha$ - $\text{Al}_2\text{O}_3$  coatings. *Surf. Coat. Technol.* **1992**, *50*, 213–222. [[CrossRef](#)]
19. Dhakar, B.; Namdeo, A.; Chatterjee, S.; Sabiruddin, K. Heat treatment of plasma sprayed alumina-chromia composite coatings. *Surf. Eng.* **2018**, *34*, 737–746. [[CrossRef](#)]
20. Caruso, K.S.; Drewry, D.G.; King, D.E.; Jones, J.S. Heat treatment of plasma-sprayed alumina: Evolution of microstructure and optical properties. In *Advanced Ceramic Coatings and Interfaces II*; Schulz, U., Lin, H.-T., Salem, J., Zhu, D., Eds.; John Wiley & Sons, Inc.: Hoboken, NJ, USA, 2007; pp. 175–192. ISBN 9780470339510.
21. Das, B.; Nath, A.K.; Bandyopadhyay, P.P. Online monitoring of laser-remelting of plasma sprayed coatings to study the effect of cooling rate on residual stress and mechanical properties. *Ceram. Int.* **2018**, *44*, 7524–7534. [[CrossRef](#)]
22. Li, C.G.; Yu, Z.S.; Zhang, Y.F.; Zhang, P.L.; Yan, H.; Lu, Q.H.; Li, W.G.; Wang, Y. Microstructure evolution of laser remelted  $\text{Al}_2\text{O}_3$ -13wt.% $\text{TiO}_2$  coatings. *J. Alloys Compd.* **2013**, *576*, 187–194. [[CrossRef](#)]
23. Wang, Y.; Li, C.G.; Tian, W.; Yang, Y. Laser surface remelting of plasma sprayed nanostructured  $\text{Al}_2\text{O}_3$ -13wt.% $\text{TiO}_2$  coatings on titanium alloy. *Appl. Surf. Sci.* **2009**, *255*, 8603–8610. [[CrossRef](#)]
24. Yuanzheng, Y.; Youlan, Z.; Zhengyi, L.; Yuzhi, C. Laser-remelting of plasma sprayed  $\text{Al}_2\text{O}_3$  ceramic coatings and subsequent wear resistance. *Mater. Sci. Eng. A* **2000**, *291*, 168–172. [[CrossRef](#)]
25. Das, B.; Gopinath, M.; Nath, A.K.; Bandyopadhyay, P.P. Effect of cooling rate on residual stress and mechanical properties of laser remelted ceramic coating. *J. Eur. Ceram. Soc.* **2018**, *38*, 3932–3944. [[CrossRef](#)]
26. Das, B.; Nath, A.; Bandyopadhyay, P.P. Scratch resistance and damage mechanism of laser remelted thermally sprayed ceramic coating. *Surf. Coat. Technol.* **2019**, *364*, 157–169. [[CrossRef](#)]
27. Sivakumar, R.; Mordike, B.L. Laser melting of plasma sprayed ceramic coatings. *Surf. Eng.* **1988**, *4*, 127–140. [[CrossRef](#)]
28. Szafarska, M.; Iwaszko, J. Laser-remelting treatment of plasma-sprayed  $\text{Cr}_2\text{O}_3$  oxide coatings. *Arch. Metall. Mater.* **2012**, *57*, 215–221. [[CrossRef](#)]
29. Conze, S.; Grimm, M.; Berger, L.-M.; Thiele, S.; Drehmann, R.; Lampke, T. Influence of simultaneous  $\text{Cr}_2\text{O}_3$  and  $\text{TiO}_2$  additions on the microstructure and properties of APS alumina coatings. *Surf. Coat. Technol.* **2021**, *405*, 126702. [[CrossRef](#)]
30. Grimm, M.; Conze, S.; Berger, L.-M.; Drehmann, R.; Lampke, T. Microstructure and properties of atmospheric plasma sprayed  $(\text{Al,Cr})_2\text{O}_3$ - $\text{TiO}_2$  coatings from blends. *J. Therm. Spray Technol.* **2022**, *31*, 256–268. [[CrossRef](#)]
31. Ghazali, M.J.; Forghani, S.M.; Hassanuddin, N.; Muchtar, A.; Daud, A.R. Comparative wear study of plasma sprayed  $\text{TiO}_2$  and  $\text{Al}_2\text{O}_3$ - $\text{TiO}_2$  on mild steels. *Tribol. Int.* **2016**, *93*, 681–686. [[CrossRef](#)]
32. Yilmaz, R.; Kurt, A.O.; Demir, A.; Tatlı, Z. Effects of  $\text{TiO}_2$  on the mechanical properties of the  $\text{Al}_2\text{O}_3$ - $\text{TiO}_2$  plasma sprayed coating. *J. Eur. Ceram. Soc.* **2007**, *27*, 1319–1323. [[CrossRef](#)]
33. Fernel, V.; Normand, B.; Coddet, C. Tribological behavior of plasma sprayed  $\text{Al}_2\text{O}_3$ -based cermet coatings. *Wear* **1999**, *230*, 70–77. [[CrossRef](#)]
34. Szkodo, M.; Bień, A.; Antoszkiewicz, M. Effect of plasma sprayed and laser re-melted  $\text{Al}_2\text{O}_3$  coatings on hardness and wear properties of stainless steel. *Ceram. Int.* **2016**, *42*, 11275–11284. [[CrossRef](#)]
35. Yang, K.; Li, J.; Wang, Q.; Li, Z.; Jiang, Y.; Bao, Y. Effect of laser-remelting on microstructure and wear resistance of plasma sprayed  $\text{Al}_2\text{O}_3$ -40% $\text{TiO}_2$  coating. *Wear* **2019**, *426–427*, 314–318. [[CrossRef](#)]